Analytical Method to Generate the Response Matrix Cross Correlations Used in the Passive Coincidence Shape Unfolding Technique for Plutonium Objects

Lisa Chiang * Richard Oberer†

Abstract

A measurement technique was developed to extract the general shape of a plutonium object containing ^{240}Pu using second order cross correlations and the nonnegative least squares (NNLS) algorithm. This technique relies on the use of a response matrix composed of the detector-detector cross correlations for four detectors arranged in a tetrahedron about the object being measured. For this work, the response matrix was empirically measured but work towards analytically generating this matrix was begun. This paper will show a method of generating the detector-detector cross correlations.

1 Introduction

In a non-multiplying and non-attenuating medium containing a spontaneous fission source such as ^{240}Pu, the detector-detector cross correlations are additive. Thus, the object can be modeled as a finite collection of point sources. This linear system can be represented mathematically as $RX = B$ where R is the response matrix, B is the set of measured cross correlations for the object, and X is the unknown shape vector. R is simply the set of empirically measured or analytically generated detector-detector cross correlations for every grid point in the volume of interest. This methodology is described in more detail in Chapter 2 of Reference [2].

*BWXT-Y12, P.O. BOX 2009 MS 8189, Oak Ridge, TN 37831-8189
†BWXT-Y12, P.O. BOX 2009 MS 8084, Oak Ridge, TN 37831-8084

2 Analytical Model of Cross Correlations

Ideally, the cross correlations can be analytically generated if one knows the probability distributions of the radiation particles emitted by the spontaneous fissioning isotope. For this study the ^{240}Pu isotope was emulated by ^{252}Cf. Since spontaneous fissioning isotopes emit both neutrons and gamma rays, the cross correlation between the *ith* and *jth* detectors, $C_{ij}(\tau_{ij})$ will be composed of four components due to the four possible coincident pairs: neutron-neutron (n,n), neutron-gamma (n,g), gamma-neutron (g,n), and gamma-gamma (g,g). Thus, $C_{ij}(\tau_{ij})$ is

$$C_{ij}(\tau_{ij}) = C_{n,n}(\tau_{ij}) + C_{n,g}(\tau_{ij}) + C_{g,n}(\tau_{ij}) + C_{g,g}(\tau_{ij}). \tag{1}$$

Each subcomponent, $C_{n,n}(\tau_{ij})$, $C_{n,g}(\tau_{ij})$, $C_{g,n}(\tau_{ij})$, and $C_{g,g}(\tau_{ij})$, can be computed from the probability distribution of the coincident pair, the source rate, multiplicities of the radiation particle, and the geometry factors between the source and each pair of detectors. Thus, $C_{ij}(\tau_{ij})$ can be computed using Equation (2) below where S is the source rate and g_i and g_j are the corresponding geometry factors for the source attenuation due to distance of the source from detectors i and j. The intrinsic detector efficiencies are not explicitly shown below because they are included in the joint probability functions $p_{n,n}$, $p_{g,g}$, $p_{n,g}$, and $p_{g,n}$. The neutron and gamma multiplicities are ν and γ, respectively.

$$\begin{aligned} C_{i,j}(\tau_{ij}) = & S g_i g_j \Big[\overline{\nu(\nu-1)} p_{n,n}(\tau_{ij}) + \overline{\nu\gamma} p_{n,g}(\tau_{ij}) + \overline{\gamma\nu} p_{g,n}(\tau_{ij}) \\ & + \overline{\gamma(\gamma-1)} p_{g,g}(\tau_{ij})\Big] \end{aligned} \tag{2}$$

All that remains to compute the detector-detector cross correlations are the form of the joint probability distribution functions: $p_{n,n}$, $p_{n,g}$, $p_{g,n}$, and $p_{g,g}$. Since the joint pdf can be computed by convolving the marginal pdfs the detector-detector cross correlation can be computed by convolving together the source-detector correlations as shown in Equations (3) to (6).

$$p_{n,n}(\tau_{ij}) = \int_{-\infty}^{\infty} p_n(-\tau_i) p_n(\tau_{ij} + \tau_i) d\tau_i \tag{3}$$

$$p_{n,g}(\tau_{ij}) = \int_{-\infty}^{\infty} p_n(-\tau_i) p_g(\tau_{ij} + \tau_i) d\tau_i \tag{4}$$

$$p_{g,n}(\tau_{ij}) = \int_{-\infty}^{\infty} p_g(-\tau_i) p_n(\tau_{ij} + \tau_i) d\tau_i \tag{5}$$

$$p_{g,g}(\tau_{ij}) = \int_{-\infty}^{\infty} p_g(-\tau_i) p_g(\tau_{ij} + \tau_i) d\tau_i \tag{6}$$

To compare an analytically generated cross correlation with a measured one, detectors 1 and 4 from the four-detector tetrahedron were used. The source-detector spacing was 36.74 cm and the peak detector efficiency for neutrons was 53.81%. The energy threshold for neutrons was 0.66 MeV.

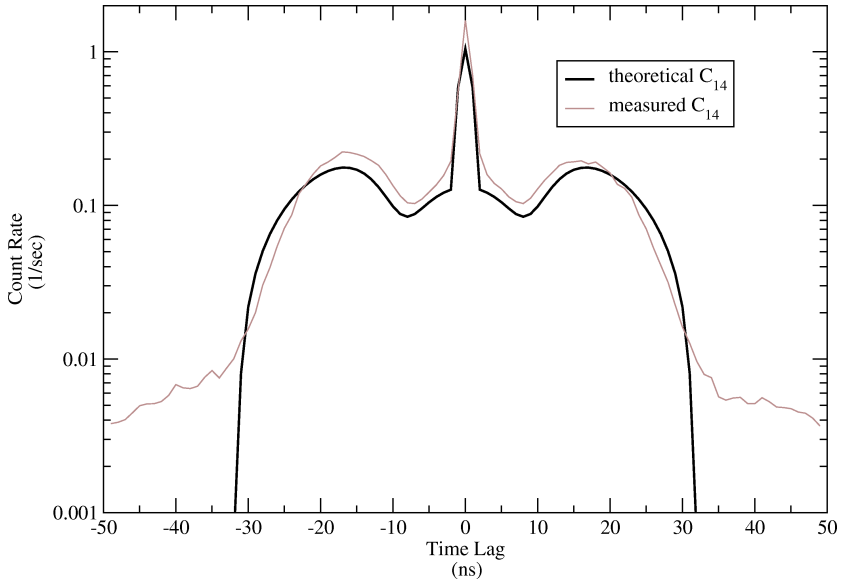

Figure 1: Comparison of theoretical and measured detector-detector cross correlations.

Figure 1 shows the measured and theoretical cross correlations. The most apparent discrepancy are the shoulders of the measured cross correlation ($\tau < -32$ ns and $\tau > 32$ ns) which are higher than the analytically generated cross correlation. This effect is primarily due to scattering processes that are not included in the analytical pdfs. Section 3 below describes how scattering effects can be included.

3 Scattering

The coincidence measurements in the laboratory include counts from accidental coincidences. There are several sources of accidental coincidences. Some sources of background produce uncorrelated counts in the detectors. Other sources though, are correlated with the source material being measured. For

example, neutrons from the spontaneous isotope can interact with the surrounding materials and produce gammas via inelastic collisions. Also, the neutrons can scatter from the surrounding materials into one of the four detectors. The correlation measurement system only removes uncorrelated background. Therefore, the analytically generated cross correlations must include scattering effects.

The scattered portions of the detector-detector cross correlation are composed of five components since the scattered particle can be coincident with either a gamma, (s,g) and (g,s), neutron, (s,n) and (n,s), or another scattered particle, (s,s). Therefore, the scattered components of the detector-detector cross correlation between detectors i and j, can be computed as shown in Equation (7) below. Note that only one geometry factor is shown for the first four components as the other geometry factor is included in the joint scattering pdfs.

$$\begin{aligned} C_{ij,scattered}(\tau_{ij}) &= C_{s,n}(\tau_{ij}) + C_{n,s}(\tau_{ij}) + C_{s,g}(\tau_{ij}) + C_{g,s}(\tau_{ij}) + C_{s,s}(\tau_{ij}) \\ &= Sg_j\overline{\nu}p_{s,n}(\tau_{ij}) + Sg_i\overline{\nu}p_{n,s}(\tau_{ij}) + Sg_j\overline{\gamma}p_{s,g}(\tau_{ij}) \\ &+ Sg_i\overline{\gamma}p_{g,s}(\tau_{ij}) + Sp_{s,s}(\tau_{ij}) \end{aligned} \tag{7}$$

One can generate the joint scattering pdfs $p_{s,n}(\tau_{ij})$, $p_{n,s}(\tau_{ij})$, $p_{s,g}(\tau_{ij})$, $p_{g,s}(\tau_{ij})$, and $p_{s,s}(\tau_{ij})$ by convolving the marginal pdfs as shown in Equations (8) to (12). Thus, the individual scattering pdfs, $p_n(\tau)$, $p_g(\tau)$, and $p_s(\tau)$ must be known. The marginal pdfs for the gamma and neutron particles were derived in Chapter 3 of Reference[2]. The marginal pdf for the scattered particles were computed using a MCNP™[1] simulation.

$$p_{s,n}(\tau_{ij}) = \int_{-\infty}^{\infty} p_s(-\tau_i)p_n(\tau_{ij} - \tau_i)d\tau_i \tag{8}$$

$$p_{n,s}(\tau_{ij}) = \int_{-\infty}^{\infty} p_n(-\tau_i)p_s(\tau_{ij} - \tau_i)d\tau_i \tag{9}$$

$$p_{s,g}(\tau_{ij}) = \int_{-\infty}^{\infty} p_s(-\tau_i)p_g(\tau_{ij} - \tau_i)d\tau_i \tag{10}$$

$$p_{g,s}(\tau_{ij}) = \int_{-\infty}^{\infty} p_g(-\tau_i)p_s(\tau_{ij} - \tau_i)d\tau_i \tag{11}$$

$$p_{s,s}(\tau_{ij}) = \int_{-\infty}^{\infty} p_s(-\tau_i)p_s(\tau_{ij} - \tau_i)d\tau_i \tag{12}$$

The simulation included the aluminum table on which the detectors rested and the floor which was modeled as a 1-foot thick slab of concrete. The table and detectors were placed at the same heights as in the lab. The total neutron and photon fluxes along with the uncollided flux in each detector was tabulated. The ^{252}Cf source was modeled as a Watt fission spectrum.

The photon portion of the source was not emulated in order to demonstrate that the resultant gamma rays are due to secondary production rather than the ^{252}Cf source itself. Coupled neutron-photon transport was turned on in the simulation. Neutrons whose energies were between 1 MeV and 17 MeV were tallied at the point detectors. Photons between 200 keV and 17 MeV were also tallied at the point detectors. Both sets of tallies were collected from 1 to 100 nanoseconds after fission. The detector count rate per fluence was calculated by dividing the total detector count rate by the total fluence at the detector. The count rate produced by scattering events was then computed by multiplying this ratio by the scattered fluence.

The marginal pdf for the scattering particle arises from either of two scattering interactions. One, a neutron can scatter in surrounding materials, such as the detector pedestal, floor, or table. Or, a gamma can be generated from a neutron inelastically scattering in the surrounding materials. Figure 2 shows the marginal pdf $p_s(\tau)$, formed from both the elastically scattered neutrons and the gammas produced from inelastic interactions.

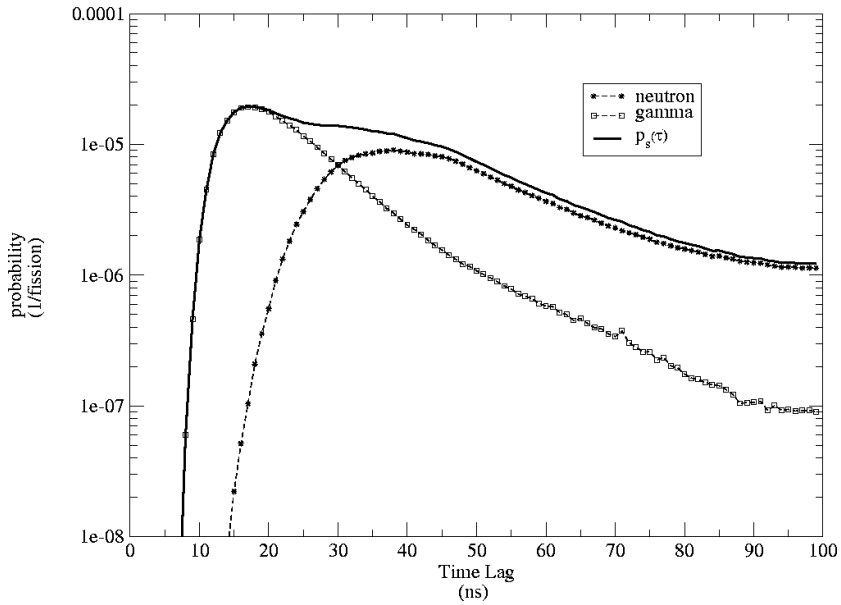

Figure 2: Marginal scattering probability density function, $p_s(\tau)$ for a source at grid point (2,2,2) and a source-detector distance of 36.74 cm.

Figure 3 shows the results of the MCNP simulation overlaid on the corresponding time-of-flight (TOF) spectrum for Detector 4. The secondary

production of gamma rays underlies the neutron distribution in the TOF. The scattered neutrons appear at time lag values greater than 20 ns which affects the tail of the neutron distribution and the apparent uncorrelated background.

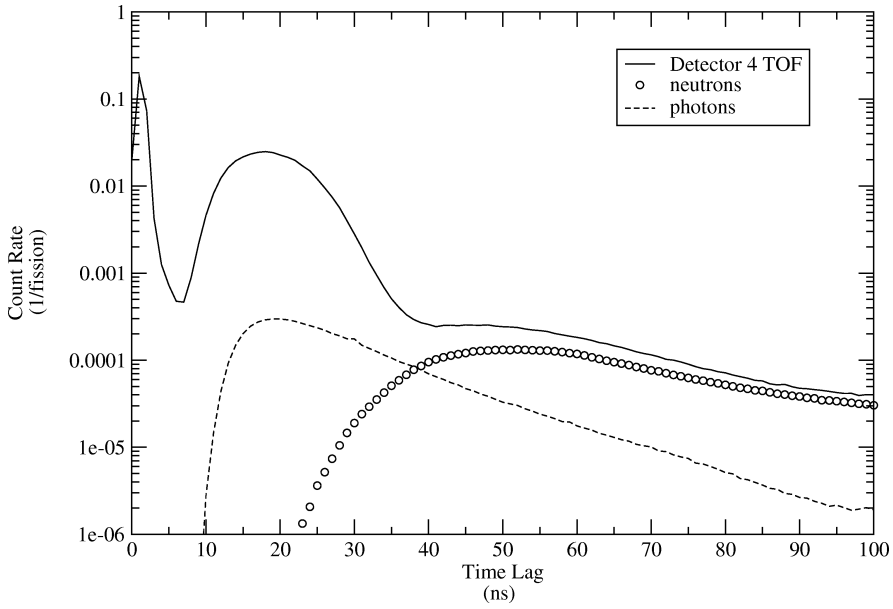

Figure 3: Calculated (MCNP) neutron and photon components of floor scattering for detector #4.

The analytic and semi-analytic detector-detector cross correlation can now be generated using

$$\begin{aligned} C_{ij}(\tau_{ij}) = {} & C_{n,n}(\tau_{ij}) + C_{n,g}(\tau_{ij}) + C_{g,n}(\tau_{ij}) + C_{g,g}(\tau_{ij}) \\ & + C_{s,n}(\tau_{ij}) + C_{n,s}(\tau_{ij}) + C_{s,g}(\tau_{ij}) + C_{g,s}(\tau_{ij}) + C_{s,s}(\tau_{ij}). \end{aligned} \tag{13}$$

All of the scattered and non-scattered components of the detector-detector cross correlation for $C_{14}(\tau_{14})$ are shown in Figure 4. The non-scattered components, $C_{g,g}(\tau_{14})$, $C_{n,g}(\tau_{14})$, $C_{g,n}(\tau_{14})$, and $C_{n,n}(\tau_{14})$ are shown as dashed lines but they are not shown in the legend of the graph.

As expected, the component due to scattering alone, $C_{s,s}(\tau_{14})$ is the smallest. In fact, it is more than two orders of magnitude smaller than $C_{n,n}(\tau_{14})$ which is not a very prominent feature in the cross correlation. The maximum

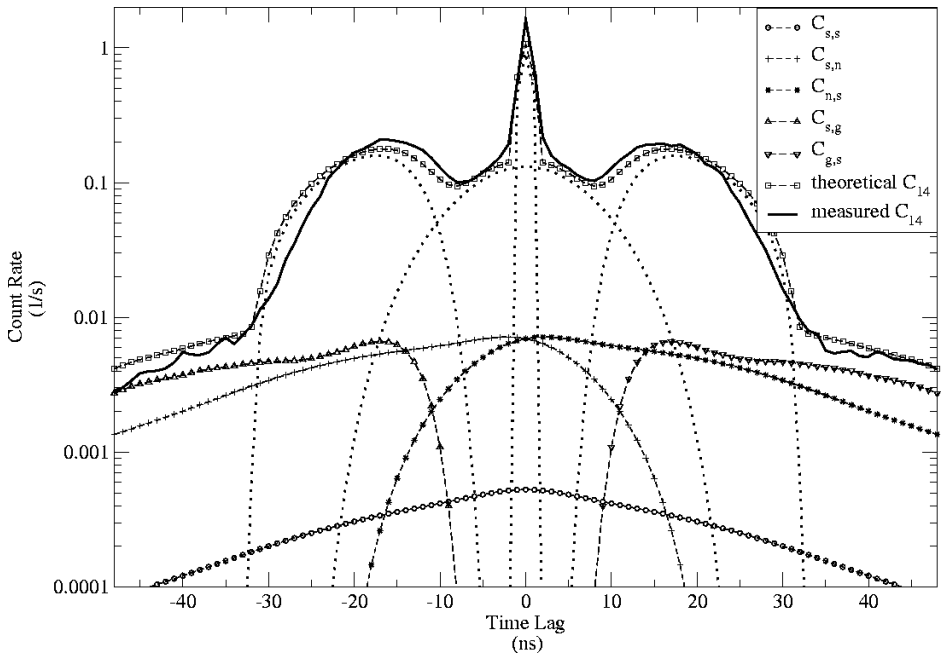

Figure 4: Scattered and non-scattered components of $C_{14}(\tau_{14})$.

amplitude of the scattering components that arise from a scattered particle being coincident with a gamma ($C_{s,g}(\tau_{14})$ and $C_{g,s}(\tau_{14})$), or with a neutron ($C_{s,n}(\tau_{14})$ and $C_{n,s}(\tau_{14})$), are an order of magnitude less than the $C_{n,n}(\tau_{14})$. In order to better understand the relative magnitudes of the component cross correlations, Table 1 shows the maximum count rate for each component in the second column and its ratio as a percentage of the maximum amplitude of the g-g peak in the last column.

In Figure 4, it is apparent that the theoretical cross correlation overestimates the number of neutrons in the region of 24 to 32 ns and -24 to -32 ns and underestimates the number of neutrons in the region -23 ns $\leq \tau \leq 23$ ns. This can probably be explained by the detector efficiency function, $\epsilon(\tau)$ being slightly incorrect for this particular source-detector distance. Since the detector efficiency is derived by assuming that the entire distribution that lies to the right of the gamma peak is solely due to neutrons, secondary processes like inelastic scattering that inject gamma detections into this region of the TOF, distort the derived neutron efficiency curve.

Table 1: Comparison of maximum amplitudes of the component cross correlations.

Cross Correlation	Maximum amplitude (counts/fission)	Percentage of $C_{g,g}$ (%)
$C_{g,g}$	0.9147	100.00
$C_{g,n}$, $C_{n,g}$	0.1581	17.28
$C_{n,n}$	0.1314	14.36
$C_{s,n}$, $C_{n,s}$	0.0072	00.78
$C_{s,g}$, $C_{g,s}$	0.0066	00.72
$C_{s,s}$	0.0005	00.06

4 Conclusions

By combining analytically and semi-analytically components of the detector-detector cross correlation, a fairly good estimate of a measured cross correlation is possible. To improve the generated cross correlation, a better model of the detector efficiency function for both neutrons and gamma rays is required. Currently, only the efficiency function for neutrons is estimated.

References

[1] Judith F. Briesmeister, editor. *MCNP™ - A General Monte Carlo N-Particle Transport Code.* Los Alamos National Laboratory, March 2000. Version 4C.

[2] L. G. Chiang. *Passive Coincidence Technique to Determine the Shape of Plutonium Objects Using Second Order Statistics.* PhD thesis, Georgia Institute of Technology, March 2002.